Triple-Mode Active-Passive Parallel Intermediate Links Converter With High Voltage Gain and Flexibility in Selection of Duty Cycles

Bhaskar, Mahajan Sagar; Almakhles, Dhafer J.; Padmanaban, Sanjeevikumar; Holm-Nielsen, Jens Bo; Kumar, A. Rakesh; Masebinu, Samson O.

Triple-Mode Active-Passive Parallel Intermediate Links Converter With High Voltage Gain and Flexibility in Selection of Duty Cycles

MAHAJAN SAGAR BHASKAR [ID]1, (Senior Member, IEEE),
DHAFER J. ALMAKHLES [ID]1, (Senior Member, IEEE),
SANJEEVIKUMAR PADMANABAN [ID]2, (Senior Member, IEEE),
JENS BO HOLM-NIELSEN [ID]2, A. RAKESH KUMAR [ID]3, (Member, IEEE),
AND SAMSON O. MASEBINU2,4

1Renewable Energy Laboratory, Department of Communications and Networks Engineering, College of Engineering,
Prince Sultan University, Riyadh 11586, Saudi Arabia
2Center for Bioenergy and Green Engineering, Department of Energy Technology, Aalborg University Esbjerg, 6700 Esbjerg, Denmark
3Department of Electrical and Electronics Engineering, National Institute of Technology Tiruchirappalli, Tiruchirappalli 620015, India
4Process Energy & Environmental Technology Station (PEETS), Faculty of Engineering and the Built Environment,
University of Johannesburg, Johannesburg 2028, South Africa

Corresponding authors: Mahajan Sagar Bhaskar (sagar25.mahajan@gmail.com) and A. Rakesh Kumar (rakesh.a@ieee.org)

ABSTRACT A high number of research work is being carried out in the field of DC-DC converters to improve the performance of microgrid operation. The DC microgrid has a high level of acceptance because of the integration of renewable energy sources. In DC Microgrid, there is a need for improved DC-DC converter topologies which offer high gain, small size, enhanced efficiency, reduced voltage stress and reduced component count etc. A new Triple-Mode Active-Passive Parallel Intermediate Links (TM-A2P-IL) converter is proposed in the paper. The A2P-IL is designed by a combination of an inductor, capacitor, diode, and control switch. The proposed converter is derived by inserting A2P-IL in conventional boost converter. The proposed TM-A2P-IL converter operates in three modes and provides a high voltage gain without using a transformer, voltage multiplier stages, coupled inductor, switched inductor/capacitor circuitry. The other benefits of the proposed TM-A2P-IL converters are flexibility in the selection of duty cycles, reduced voltage stress of devices, small reactive components, single-stage power conversion. The proposed converter circuit, operating principle, steady-state analysis is studied for both CCM and DCM, discussed. The comparison between available similar type converters and the proposed converter is provided. The operation and performance of the proposed A2P-IL converter are validated through simulation and experimental work.

INDEX TERMS Active-passive links, boost converter, DC microgrid, high voltage gain, parallel intermediate links, reduced voltage stress.

I. INTRODUCTION

Renewable Energy Sources (RES) are increasingly replacing conventional and fossil fuels because of their depleting nature and contribution to global warming. The solar power is found abundantly in nature; hence, PV power is seen as a welcome revolution. This has given rise to the evolution of microgrid,

The associate editor coordinating the review of this manuscript and approving it for publication was Eklas Hossain [ID].

which consists of different Distributed Energy Resources (DER) and interconnected loads with established control entity to manage the network [1], [2]. Fig. 1 shows the typical structure of DC microgrid. There is also seen an increased number of loads operating on DC power.

With the PV power generating DC output and loads operating on DC power, DC microgrid has caught the attention of various governments, academicians and researchers [3], [4]. DC output power converter with high efficiency and high
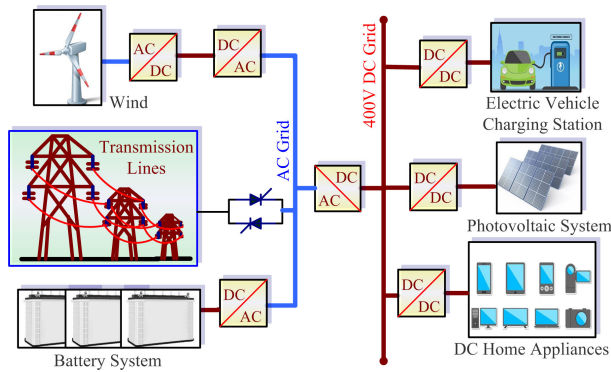
FIGURE 1. General 400V DC Microgrid system.

voltage gain is necessary to integrate renewable into a micro-grid. The DC-DC converters can be classified into isolated and non-isolated converters [5]. The isolated converter uses a transformer and coupled inductors where voltage gain depends on turns ratio or coupling factor. However, there are many disadvantages include leakage inductance resulting in voltage spikes, increased converter's inductance value with an increase in voltage gain.

The cost of the transformer also puts an additional burden on the total cost of the converter [6], [7]. The coupled inductors-based converter offers a higher gain with an increase in the coupling factor. This provides proper voltage regulation, but the leakage inductance has its adverse effect on switch voltage stress and additionally clamp circuitry is required for these converters [8], [9]. On the other hand, there are many benefits to employing a non-isolated converter. With the elimination of the transformer, it reduces the cost and size of the converter [10], [11]. This also makes the converter circuit simpler in topology. A conventional boost converter is the most basic form of the step-up converter, but it encounters the diode reverse recovery problem when converter operates at a high duty cycle to achieve high voltage gain. The conventional boost converters, when operated under extreme duty ratio, do not provide the sufficient duration of time to transfer the energy stored in the inductor to the capacitor. The other drawbacks of the classical boost converter are reduced efficiency at a higher duty cycle, voltage stress across devices, high input current rating, electromagnetic interference, reverse recovery of the diode, low efficiency at a higher duty cycle, etc. [12], [13]. The quadratic boost converters offer high voltage gain by using two stages of classical converters. However, required higher rating devices and reactive components, the problem of reverse recovery with the diodes persist and also require accurate control because of non-linear voltage gain [14], [15]. The cascaded boost converters employ to increase the gain to the required level. However, this comes at the cost of an increased number of components which makes the circuit expensive, complicated and bulky [16], [17].

Moreover, the rating of components and devices are increasing with the number of cascaded stages. The interleaved boost converter topologies offer reduced input current ripples. However, the voltage gain of this topology is similar to a conventional boost converter [18].

Recently, the interleaved structure is used along with diode-capacitor stages to attain higher voltage gain. Nevertheless, these converters required a large number of diode and capacitors at the output side [19]–[22]. The Switched Capacitor (SC) type converter presents a more straightforward structure with reduced voltage stress across switches. However, these structures have low efficiency and required a large number of power devices and capacitors, and mainly suitable for low power application [23], [24]. The conventional converters could be integrated with voltage multiplier cells to increase the gain and reduces the maximum voltage across the switches. However, the power handling capability is limited, and the circuit is complicated due to the requirement of a large number of diode-capacitor multiplier stages [25]–[28]. The concept of voltage lift is used in the converter presented in [29], [30]. The converter is relatively simple in structure with minimum switches resulting in reduced cost. It also offers the least possible voltage ripple and high efficiency. Charging the inductor in parallel and discharging the inductor in series is a usual way to improve the voltage gain [31], [32]. In [33], voltage gain is slightly improved by using two switches and additional diode and capacitor circuitry. In [34]–[36], two different duty cycles are used to achieve a higher voltage gain. The converter is a non-isolated version and suitable for microgrid application. However, the voltage gain is not significantly improved, even using three switches and switched inductor technique. A higher voltage gain is possible with the use of active-passive inductor cells [37]. Active-passive inductor cells are integrated to increase the voltage gain. The inductor cells are replaced by switched inductor cells to increase the voltage gain [38]. However, this converter is operated with a single duty cycle, and the efficiency is severely affected because of repeated loops of energy transfer within the converter circuit. Moreover, the power circuitry required a high number of diodes and inductors, which increases the cost and size of the converter.

The proposed Triple-Mode Active-Passive Parallel Intermediate Links (TM-A2P-IL) converter is useful to overcome the drawbacks above. The TM-A2P-IL converter derived by inserting parallel A2P-IL in classical boost converter to achieve a high voltage gain. Moreover, the two-duty cycle control possible for the proposed converter, which provides flexibility in the selection of duty cycles for control switches. The proposed converter does not use any voltage multiplier circuit, switched capacitor units, switched inductor units, and transformers. The A2P-IL converter is modular and scalable to any number of stages. The proposed converter is offered a solution to achieve high voltage gain with flexibility in the selection of duty cycle for DC microgrid applications. The organization of the paper is described as follows: Section II deals with the primary circuit of the proposed A2P-IL converter, CCM and DCM characteristics waveforms, and voltage gain analysis. The design equations and
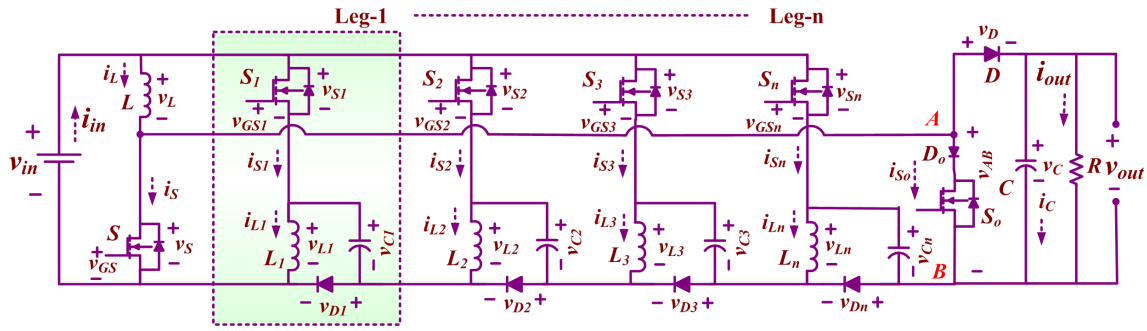
FIGURE 2. Power circuit of TM-A2P-IL converter.

comparison are presented in Section III. The simulation and experimental results are presented with suitable discussion in Section IV. At last, the conclusion is given in Section V.

II. TRIPLE-MODE ACTIVE-PASSIVE PARALLEL INTERMEDIATE LINKS (TM-A2P-IL) CONVERTER

A. POWER CIRCUIT OF TM-A2P-IL CONVERTER

The circuit diagram of the proposed TM-A2P-IL converter is shown in Fig. 2. The proposed TM-A2P-IL converter is derived by modification in the power circuit of the conventional boost converter. The conventional boost converter consists of a switch (S), inductor (L), the diode (D) and capacitor (C). The modification is carried out by inserting a set of n parallel legs within the conventional boost converter, as shown in Fig. 2. Each A2P-IL consists of a closed circuit consisting of an inductor, a capacitor, and a diode with the addition of a control switch over the top. To obtain flexibility in duty cycle and high voltage gain, a unidirectional switch S_o is added together with the diode D_o in series with it. Ideal switch, inductors and capacitors are considered to explain the operation of the proposed TM-A2P-IL converter. It is also assumed that the switches S, S_1,..., and S_n are operated with a duty cycle of q_1, while the switch S_o is operated with the duty cycle of q_2. The addition of duty cycles $q_1 + q_2$ is kept at less than unity, i.e. $q_1 + q_2 < 1$. It is also to be noted that the switch S_o is operated after turned off the remaining switches. Hence, the delay time of switch S_o is $q_1 T$, where T is the total time period.

B. CONTINUOUS CONDUCTION MODE

The waveform of the TM-A2P-IL converter during CCM is shown in Fig. 3. The proposed converter performs three modes of operation as explain as follows,

1) I^{ST} MODE OF OPERATION (Time T_0 TO T_a)

Fig. 4(a) presents the circuit diagram for the I^{st} mode of operation. Gate pulses are provided to the switches S, S_1, S_2 ..., and S_n, while the switch S_o is turn OFF with the gate pulse. During this mode, the inductors (L, L_1, L_2 ..., and L_n) and capacitors (C_1, C_2 ..., and C_n) are charged by the voltage source v_{in}. The diode D is reverse biased and diodes (D_1, D_2 ..., and D_n) are forward biased. Therefore, all the inductors and capacitors of A2P-IL legs are charged in parallel. The voltages across inductors L, L_1, L_2 ..., and L_n are obtained as,

$$v_L, v_{L1}, v_{L2} \ldots, v_{Ln}\} \approx V_{in} \qquad (1)$$

where V_{in} is the average input voltage. The voltage across capacitors C, C_1, C_2 ..., and C_n are obtained as,

$$v_{C1}, v_{C2} \ldots, v_{Cn}\} \approx V_{in}; \quad v_C \approx V_{out} \qquad (2)$$

where V_{out} is the average output voltage. The current through inductor L and capacitor C can be obtained as,

$$i_L = i_{in} - \left(\sum_{w=1}^{n} i_{Cw} + \sum_{v=1}^{n} i_{Lv} \right), \quad i_C = -i_{out} \approx -\frac{V_{out}}{R} \qquad (3)$$

The ripples in the inductors currents for this mode are calculated as follows,

$$\left\{ \Delta i_L^I = \frac{V_{in}T}{L}q_1, \Delta i_{L1}^I = \frac{V_{in}T}{L_1}q_1, \cdots, \Delta i_{Ln}^{~I} = \frac{V_{in}T}{L_n}q_1 \right. \qquad (4)$$

The inductance rating of the all the inductor are same, therefore, (4) is rewritten as,

$$\Delta i_L^I = \Delta i_{L1}^I = \cdots = \Delta i_{Ln}^{~I} = \frac{V_{in}T}{L}q_1 = \frac{V_{in}T}{L_1}q_1 = \frac{V_{in}T}{L_n}q_1 \qquad (5)$$

2) IInd MODE OF OPERATION (Time T_a TO T_b)

Fig. 4(b) presents the circuit diagram for the IInd mode of operation. The switch S_o is turn ON, while the remaining switches (S, S_1, S_2 ..., and S_n) are turned OFF. The diodes (D_1, D_2 ..., and D_n) that were previously forward-biased are now reverse biased. However, the diode D continues to be reverse biased during this mode. The inductors are now charged in series by capacitor voltages and input voltage. The inductor and capacitor voltages are related as follows,

$$\begin{cases} v_L + v_{Ln} + . + v_{L2} + v_{L1} \approx V_{in} + v_{Cn} + . + v_{C2} + v_{C1} \\ v_L + \sum_{v=1}^{n} v_{Lv} \approx \sum_{w=1}^{n} v_{Cw} + V_{in} \end{cases} \qquad (6)$$

The voltage across capacitors C, C_1, C_2 ..., and C_n are obtained as,

$$v_{C1}, v_{C2} \ldots, v_{Cn}\} \approx V_{in}; \quad v_C \approx V_{out} \qquad (7)$$

By using (6) and (7), the voltages across inductors L, L_1, L_2 ..., and L_n are obtained as,

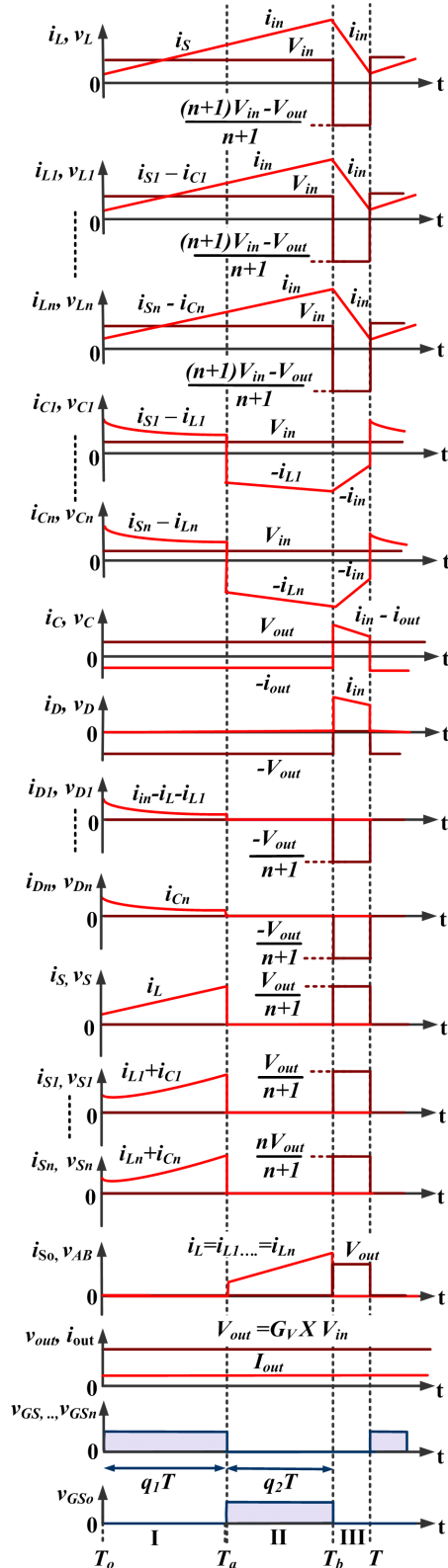$$v_L, v_{L1}, v_{L2}, \cdots, v_{Ln}\} \approx V_{in} \qquad (8)$$

FIGURE 3. Waveforms of voltage and current across/through components and devices for CCM.

The current through inductor L and capacitor C can be obtained as,

$$i_L = i_{in}, i_C = -i_{out} \approx -\frac{V_{out}}{R} \qquad (9)$$

The ripples in the inductor currents for this mode are calculated as follows,

$$\begin{cases} \Delta i_L^{II} = \frac{V_{in}T}{L}q_2, \Delta i_{L1}^{II} = \frac{V_{in}T}{L_1}q_2, \cdots, \Delta i_{Ln}{}^{II} = \frac{V_{in}T}{L_n}q_2 \end{cases} \qquad (10)$$

The inductance rating of the all the inductor are same, therefore, (10) is rewritten as,

$$\Delta i_L^{II} = \Delta i_{L1}^{li} = \cdots = \Delta i_{Ln}{}^{II} = \frac{V_{in}T}{L}q_2 = \frac{V_{in}T}{L_1}q_2 = \frac{V_{in}T}{L_n}q_2 \qquad (11)$$

3) IIIrd MODE OF OPERATION (Time T_b TO T_c)

Fig. 4(c) presents the circuit diagram for the IIIrd mode of operation. All the switches (S, S_o, S_1, S_2 …, and S_n) are turn OFF during this period. The diode D, which was reverse biased for mode I and II is forward biased now. The diodes (D_1, D_2 …, and D_n) continue to be in a reverse-biased state. The energies that were build-up by the inductors and capacitors of A2P-IL legs during the mode I and II are released to the capacitor C and load R. The inductor and capacitor voltages are related as follows,

$$\begin{cases} v_L + v_{Ln} + . + v_{L1} \approx V_{in} - V_{out} + v_{Cn} + . + v_{C2} + v_{C1} \\ v_L + \sum_{v=1}^{n} v_{Lv} \approx \sum_{w=1}^{n} v_{Cw} + V_{in} - V_{out} \end{cases} \qquad (12)$$

where V_{out} is the average output voltage. The voltage across capacitors C, C_1, C_2, …, and C_n are obtained as,

$$v_{C1}, v_{C2} \ldots, v_{Cn}\} \approx V_{in}; \quad v_C \approx V_{out} \qquad (13)$$

By using (12) and (13), the voltages across inductors L, L_1, L_2 …, and L_n are obtained as,

$$v_L, v_{L1}, v_{L2}, \cdots, v_{Ln}\} \approx \frac{(n+1)V_{in} - V_{out}}{n+1} \qquad (14)$$

The current through inductor L and capacitor C can be obtained as,

$$i_L = i_{in}, i_C = i_{in} - i_{out} \approx i_{in} - \frac{V_{out}}{R} \qquad (15)$$

The ripples in the inductor currents are calculated as follows,

$$\begin{cases} \Delta i_L^{III} = \frac{((n+1)V_{in} - V_{out})T}{(n+1)L}(1 - q_1 - q_2) \\ \Delta i_{L1}^{III} = \frac{((n+1)V_{in} - V_{out})T}{(n+1)L_1}(1 - q_1 - q_2) \\ \cdots, \Delta i_{Ln}{}^{III} = \frac{((n+1)V_{in} - V_{out})T}{(n+1)L_n}(1 - q_1 - q_2) \end{cases} \qquad (16)$$

The inductance rating of the all the inductor are same, therefore, (16) is rewritten as,

$$\begin{cases} \Delta i_L^{III} = \cdots \Delta i_{Ln}{}^{III} = \frac{((n+1)V_{in} - V_{out})T}{(n+1)L}(1 - q_1 - q_2) \\ \cdots = \frac{((n+1)V_{in} - V_{out})T}{(n+1)L_n}(1 - q_1 - q_2) \end{cases} \qquad (17)$$
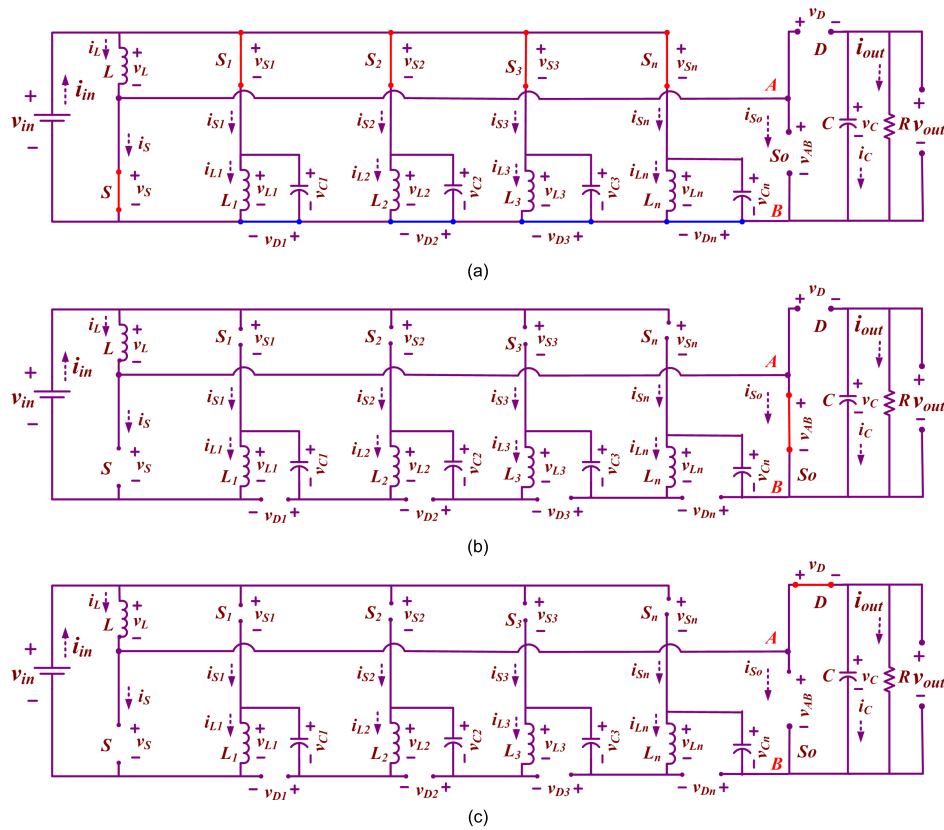
FIGURE 4. Equivalent circuitry of A2P-IL converter (a) Ist Mode ($T_o - T_a$), (b) IInd Mode ($T_a - T_b$), and (c) IIIrd Mode ($T_b - T_c$).

During CCM, the voltage gain of A2P-IL converter is obtained as,

$$G_V\rangle_{CCM} \ or \ G_V = \frac{V_{out}}{V_{in}}\bigg|_{CCM} = \frac{n+1}{1-q_1-q_2} \quad (18)$$

C. DISCONTINUOUS CONDUCTION MODE

The waveform of the TM-A2P-IL converter for DCM is shown in Fig. 5. The proposed converter performs four modes of operation as explain as follows,

1) Ist MODE OF OPERATION (Time T$_0$ TO T$_a$)

This mode of operation is similar to that of I^{st} mode of operation of CCM and follows the same equivalent power circuit. The inductors (L, L_1, L_2, …, and L_n) carry currents which increase linearly, and their maximum values are obtained as follows,

$$I_L\rangle_{\max-I} = V_{in}\frac{q_1T}{L}, \cdots, I_{Ln}\rangle_{\max-I} = V_{in}\frac{q_1T}{L_n} \quad (19)$$

The inductor currents reach the maximum value at the time $t = q_1T$, and the voltage across all the inductors are same. Therefore,

$$I_L\rangle_{\max-I} = I_{L1}\rangle_{\max-I}, \cdots, I_{Ln}\rangle_{\max-I} \quad (20)$$

2) IInd MODE OF OPERATION (Time T$_a$ TO T$_b$)

This mode of operation is similar to that of IInd mode of operation of CCM and follows the same equivalent

power circuit. The current continues to increase linearly and the maximum values of mode II are obtained as follows,

$$I_L\rangle_{\max-II} = (q_1+q_2)\frac{V_{in}T}{L}, \cdots, I_{Ln}\rangle_{\max-II}$$
$$= (q_1+q_2)\frac{V_{in}T}{L_n} \quad (21)$$

The inductor currents reach the maximum value for mode II at the time $t = q_1T + q_2T$ and the voltage across all the inductors are same. Therefore,

$$I_L\rangle_{\max-II} = I_{L1}\rangle_{\max-II}, \cdots = I_{Ln}\rangle_{\max-II} \quad (22)$$

3) IIIrd MODE OF OPERATION (Time T$_b$ TO T$_c$)

This mode of operation is similar to that of IIIrd mode of operation of CCM and follows the same equivalent power circuit. The current through the inductors reduces linearly to reach the zero value at time $t = q_1T + q_2T + q_3T$. The expression for the maximum value of inductor currents in this mode is as follows,

$$\begin{cases} I_L\rangle_{\max-III} = \dfrac{(V_{out}-(n+1)V_{in})}{(n+1)}\dfrac{q_3T}{L}, \\ \cdots, I_{Ln}\rangle_{\max-III} = \dfrac{(V_{out}-(n+1)V_{in})}{(n+1)}\dfrac{q_3T}{L_n} \end{cases} \quad (23)$$

The inductor currents reach the zero value at the time $t = q_1T + q_2T + q_3T$, and the voltage across all the inductors are same. Therefore,

$$I_L\rangle_{\max-III} = I_{L1}\rangle_{\max-III}, \cdots = I_{Ln}\rangle_{\max-III} \quad (24)$$
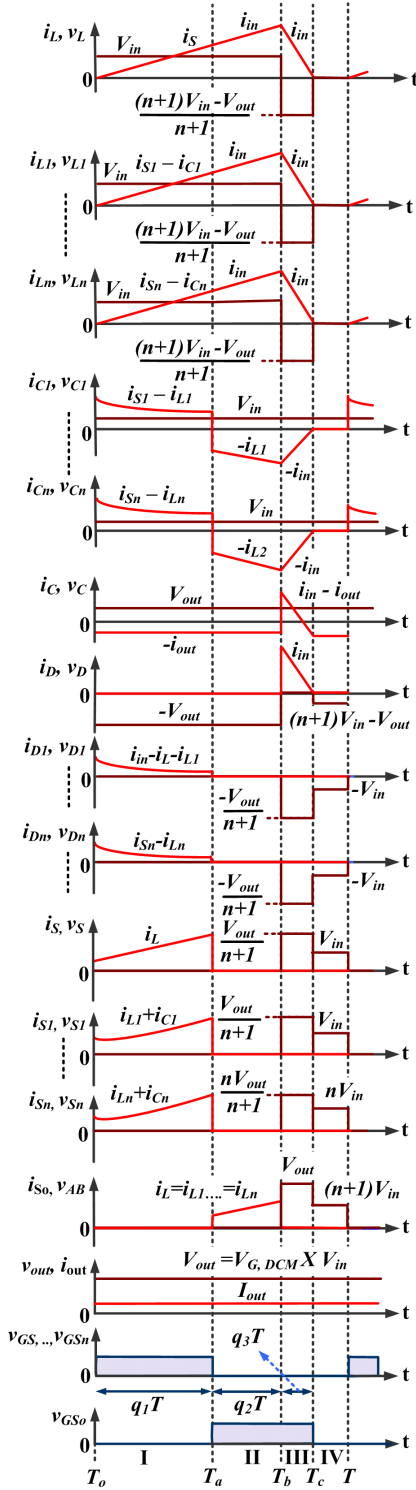
FIGURE 5. Waveforms of voltage and current across/through components and devices for DCM.

4) IVth MODE OF OPERATION (TIME T_c TO T)
The equivalent circuit of IVth mode of operation is shown in Fig. 6. During this mode, all the switches in the circuit have their gate pulses OFF, and all the diodes are reverse biased. The stored energy in the output capacitor C is delivered to the load R.

With the help of (21) and (23), the value of q_3 is obtained as follows,

$$q_3 = \frac{(q_1 + q_2)(n+1)V_{in}}{v_{out} - (n+1)V_{in}} \quad (25)$$

The capacitor C average current can be expressed as,

$$I_{Co} = \frac{V_{in}^2 (q_1 + q_2)^2 (n+1) T}{2 (Vout - (n+1) V_{in}) L} - \frac{V_{out}}{R} \quad (26)$$

The average current through any capacitor is zero. Therefore, the (26) is rewritten as follows,

$$\frac{V_{in}^2 (q_1 + q_2)^2 (n+1) T}{2 (Vout - (n+1) V_{in}) L} - \frac{V_{out}}{R} = 0 \quad (27)$$

The voltage gain of the TM-A2P-IL converter for DCM is derived as follows,

$$G_V\rangle_{DCM} = \frac{V_{out}}{V_{in}}\Bigg|_{DCM} = \frac{n+1}{2}$$
$$+ \sqrt{\frac{(n+1)^2}{4} + \frac{(q_1 + q_2)^2 (n+1)}{2\psi_L}} \quad (28)$$

where, Ψ_L is normalized inductors time constant, and it is equated to $fL/T = fL_1/R = \ldots = fL_n/R$.

The expression for boundary normalized inductor time constant Ψ_{LB} is obtained as,

$$\psi_{L-B} = \frac{(q_1 + q_2) (1 - q_1 - q_2)^2}{2 (n+1)} \quad (29)$$

The CCM and DCM regions are marked in the plot of Ψ_{L-B}, which is shown in Fig. 7. The following conditions must be satisfied in order to operate the A2P-IL converter in CCM.

$$\frac{(q_1 + q_2) (1 - q_1 - q_2)^2}{2 (n+1)} \prec \left(\frac{fL}{R} = \frac{fL_1}{R} = \cdots = \frac{fL_n}{R} \right) \quad (30)$$

III. DESIGN AND COMPARISON
A. DESIGN OF TM-A2P-IL CONVERTER
The design of TM-A2P-IL converter is carried out by considering the parameters input voltage (V_{in}), output voltage (V_{out}), output power (P_{out}), load (R) and time period (T).

By using the following equation, the duty cycle is calculated,

$$\left.\begin{array}{l} G_V = \dfrac{V_{out}}{V_{in}} = \dfrac{n+1}{1 - q_1 - q_2} = \dfrac{1}{1 - Q_{TM-A2P-IL}(q_1, q_2)} \\ Q_{TM-A2P-IL}(q_1, q_2) = (n + q_1 + q_2) / (n+1) \end{array}\right\} \quad (31)$$

Worst efficiency (η_{worst}) is considered, and the duty cycle function at worst converter efficiency is,

$$Q_{TM-A2P-IL}(q_1, q_2) = \frac{G_V - \eta_{worst}}{G_V} \quad (32)$$

The following equation is used to calculate the critical inductances (L_C) and the associated critical current rating of the inductor (I_{Lc}),

$$L_c = \frac{(q_1 + q_2) V_{in}}{f \times \Delta i_L} = \frac{(q_1 + q_2) V_{in}}{f \times 30\% of I_L}, \quad I_{Lc} > I_L + 0.5\Delta i_L \quad (33)$$
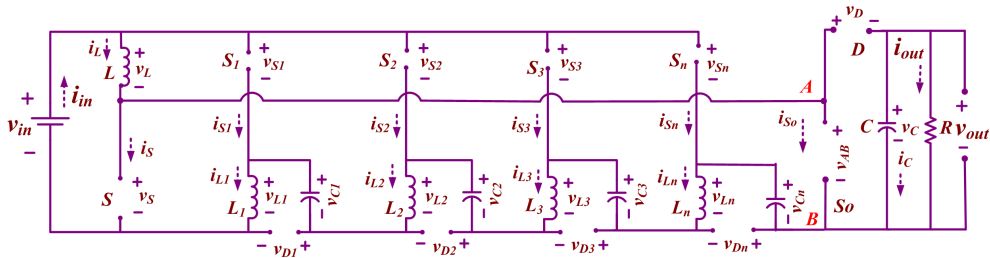
FIGURE 6. Equivalent circuitry of A2P-IL converter in DCM (T_c-T).

TABLE 1. Comparison of A2P-IL converter with classical and recently proposed converters.

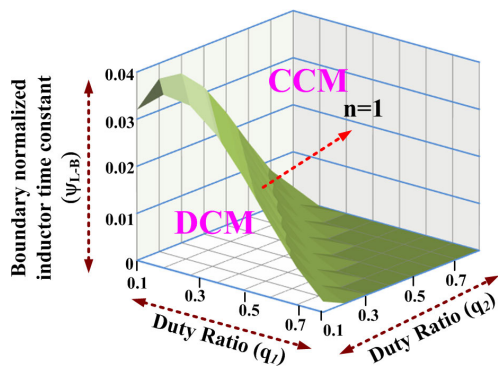| Parameters	CB	[32] (Con. I)	[32] (Con. II)	[32] (Con. III)	[34]	[37]	[38]	Proposed converter
Voltage gain, V_G	$\dfrac{1}{1-q}$	$\dfrac{q+1}{1-q}$	$\dfrac{2}{1-q}$	$\dfrac{3-q}{1-q}$	$\dfrac{1-q_1}{1-q_1-q_2}$	$\dfrac{1+(n+1)q}{1-1}$	$\dfrac{1+(2n+3)q}{1-q}$	$\dfrac{n+1}{1-q_1-q_2}$
Maximum voltage across switch (Normalized)	1	$\dfrac{V_G+1}{2V_G}$	$\dfrac{1}{2}$	$\dfrac{V_G-1}{2V_G}$	$V_{S1}=\dfrac{V_G+1}{2V_G}$ $V_{S2}=1$	$V_S=\dfrac{(n+1)+V_G}{(n+2)V_G},$ $V_{Sj}=\dfrac{(n+2-j)+jV_G}{(n+2)V_G},\ldots$	$V_S=2\dfrac{(n+1)+V_G}{(2n+4)V_G},$ $V_{Sj}=2\dfrac{(n-j+2)+jV_G}{(2n+4)V_G},\ldots$	$V_S=\dfrac{1}{n+1}$ $V_{Sj}=\dfrac{j}{n+1}$
Maximum Voltage across intermediate diode (Normalized)	-	-	$-\dfrac{1}{2}$	$-\dfrac{V_G-1}{2V_G}$	$-\dfrac{1}{V_G}$	$V_{Dj1}=-1/V_G,$ $V_{Dj2}=\dfrac{1-V_G}{(n+2)V_G}$	$V_{Dj1,\,Dj4}=-1/V_G$ $V_{Dj2}=\dfrac{-(V_G-1)}{(n+2)V_G}$ $V_{Dj3,\,Dj5}=\dfrac{-(V_G-1)}{(2n+4)V_G}$	$D_1=\dfrac{-1}{n+1}$ $D_2=\dfrac{-1}{n+1},\ldots$ $D_n=\dfrac{-1}{n+1}$
Maximum Voltage across output diode (Normalized)	-1	$-\dfrac{V_G+1}{V_G}$	-1	$-\dfrac{V_G-1}{V_G}$	$-\dfrac{V_G+1}{V_G}$	$-\dfrac{V_G+1}{V_G}$	$-\dfrac{V_G+1}{V_G}$	-1
Switches	1	2	2	2	3	n+2	n+2 (1 switch/leg)	n+2 (1 switch/leg)
Inductors	1	2	2	2	2	n+2	2n+4 (2 inductors/leg)	n+1 (1 inductor/leg)
Capacitors	1	1	2	3	1	1	1	n+1 (1 switch/leg)
Diodes	1	1	2	3	2	2n+1	5n+6 (5 diode/leg)	n+2 (1 diode/leg)
Flexibility in duty cycle	X	X	X	X	√	X	X	√

FIGURE 7. Plot of β_{LB} versus duty cycle k_1 and k_2.

where, Δi_L is assumed to be 30% of the average inductor current (I_L).

The voltage rating and critical capacitances of C_1, $C_2\ldots$, and C_n is calculated as below,

$$C_1 = C_2. = C_n = \dfrac{(1-q_1-q_2)\,I_{in}}{f \times \Delta V_C},$$
$$V_{C1} = V_{C2} = . = V_{Cn} \geq V_i \quad (34)$$

The voltage rating and critical capacitance of C_o is calculated as follows,

$$C_o = \dfrac{(q_1+q_2)V_{out}}{\Delta V_{Co} \times R \times f} = \dfrac{(k_1+k_2)V_{out}}{R \times f \times 1\% of V_o}, \quad VC_o \geq V_{out} \quad (35)$$

The voltage rating of switches S, S_o, S_1, …, and S_n can be obtained as,

$$V_S = V_{S1} = \dfrac{V_{out}}{n+1}; \quad V_{Sj(j=2,3\ldots,n)} = \dfrac{jV_{out}}{n+1}; \quad V_{So} > V_{out} \quad (36)$$

The diodes D, D, D_1, …, and D_n voltage ratings can be arrived as,

$$V_{D1} = V_{D2} = \ldots = V_{Dn} = \dfrac{-V_{out}}{n+1}; \quad V_D = -V_{out} \quad (37)$$

B. COMPARISON

Table 1 presents the comparison between the proposed and available similar converter configurations. A conventional boost converter is modified in [32], [34]. The active switched
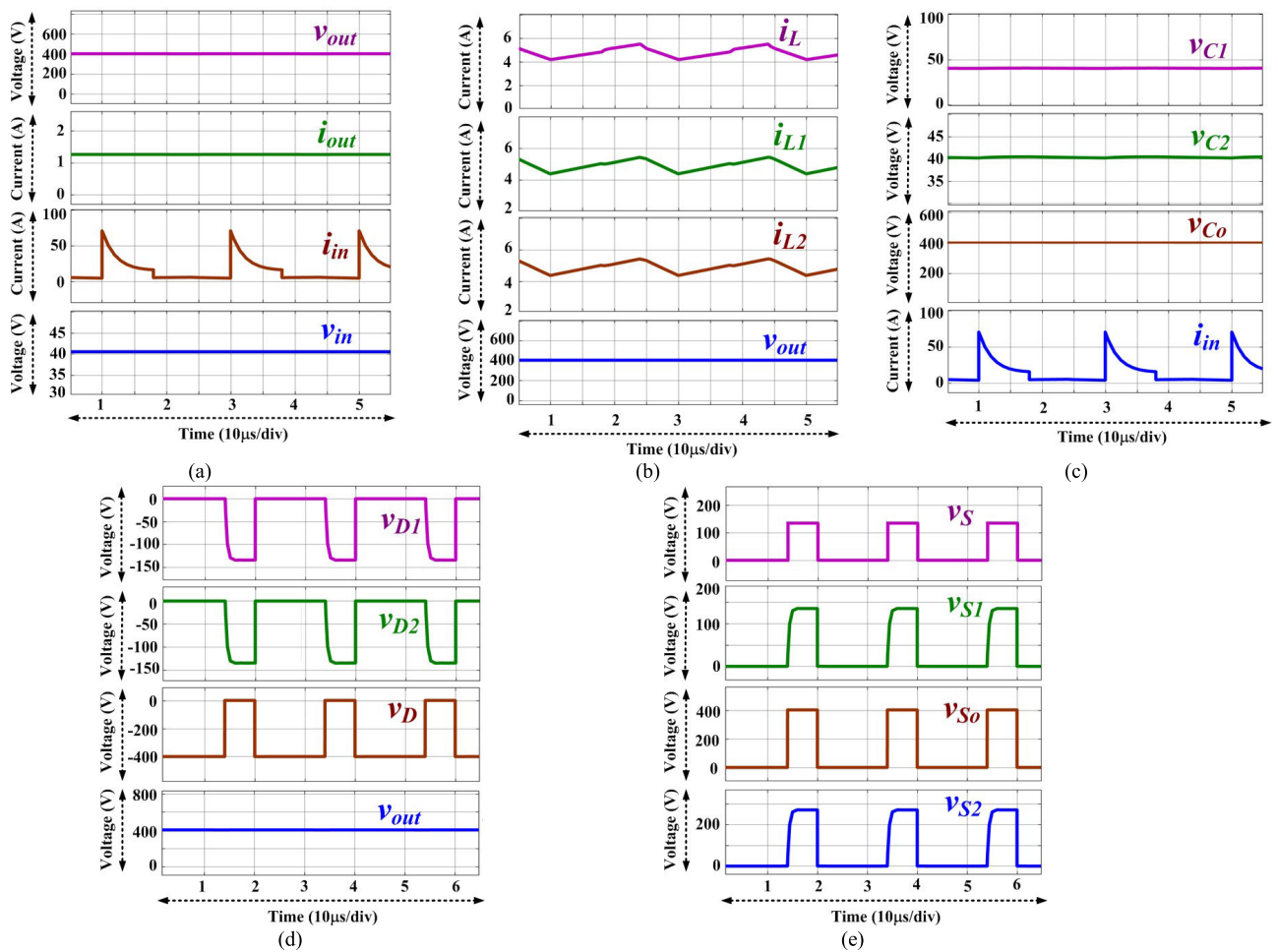
FIGURE 8. Simulation results (a) Voltage and current at input and output terminal, (b) inductor current and Output voltage, (c) Voltage across capacitor and input current, (d) Voltage across diodes and output voltage, (e) Voltage across switches.

inductor techniques and voltage life techniques are incorporated in the new leg added with the conventional boost converter. The converters presented in [37], [38] and the proposed TM-A2P-IL converters carry multi-leg structure feature which allows for selection of multiple numbers of legs. Only one switch is required for each leg. However, the converter presented in [38] employs 2 inductors and 5 diodes for each leg in addition to the single switch. The proposed converter requires only 1 capacitor, 1 diode and 1 inductor, which significantly reduce the component count. The selection of a flexible duty cycle range offers a high voltage gain. This can be achieved by employing multiple numbers of switches rather than a single switch. The conventional boost converters and the converters presented in [32] precisely suffer from the problem of limited voltage gain problem. The proposed A2P-IL converter and presented converter in [34] offer a flexible selection of duty cycle range with the help of two different duty cycles. Hence, by operating the converter with two different duty cycles, the converter can effectively offer high voltage gain. The TM-A2P-IL converter undergoes a lower normalized voltage stress compared to the converters [32], [34], [37], [38]. This enables the use of a semiconductor switch by the proposed converter with a low

voltage rating. As the number of legs increase, the voltage stress on the switches reduces, which is a striking feature of TM-A2P-IL converter. The additional switch in the TM-A2P-IL converter is enabling the operation of the converter with two different duty cycles. The additional switch also undergoes only minimum voltage stress than the output voltage. In the proposed converter, the diode at the output side has lower voltage stress compared to the output diode of converter [34], [37], [38]. Hence, it can be observed clearly that the proposed TM-A2P-IL converter offers many advantages over the other converters in the literature by providing higher voltage gain and flexibility in the selection of duty cycle for switches.

IV. SIMULATION AND EXPERIMENTAL RESULTS
Initially, to investigate the performance and theoretical analysis of the converter, the proposed converter is tested through simulation work. The converter with 2 A2P-IL is simulated by considering the parameters output reference voltage 400V, input voltage 40V, output power 500W, and switching frequency 50kHz. The inductance of 700 μH is selected for each leg and capacitance for each leg is equal to 220 μF. The output capacitance is 220μF. The switches S, S_1, and S_2 operated
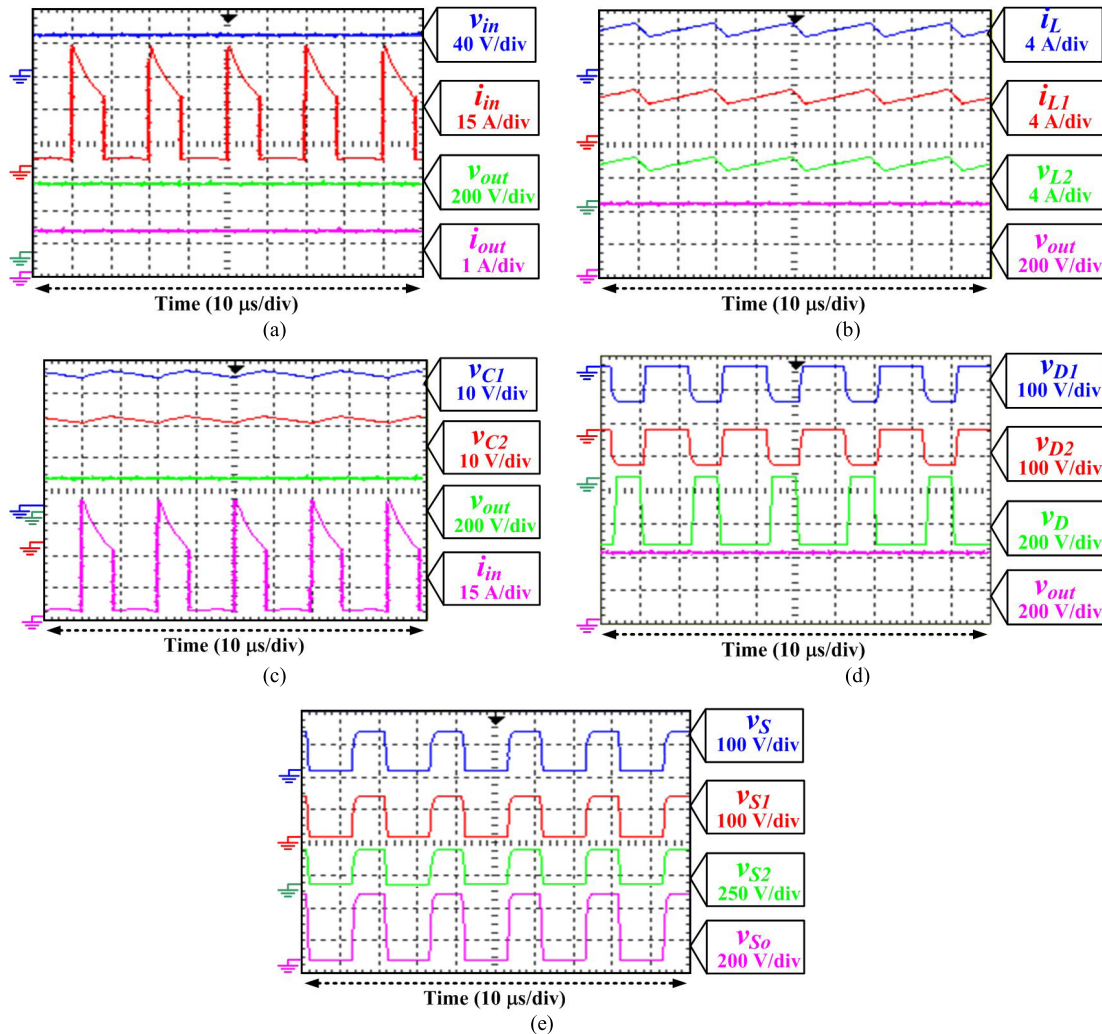
FIGURE 9. Experimental results (a) Voltage and current at input and output terminal, (b) inductor current and Output voltage, (c) Voltage across capacitor and input current, (d) Voltage across diodes and output voltage, (e) Voltage across switches.

in 180° phase shift switch S_o. The observed simulation results are shown in Fig. 8. In Fig. 8(a), the voltage and current at the input and output port are shown. It is observed that 400.3V is achieved at the output port when the input voltage is 40V. The average values of output and input current are 1.25A and 12.87A, respectively.

The inductors L, L_1 and L_2 current and output voltage waveforms are shown in Fig. 8(b). It is observed that in mode I and II, inductors L, L_1 and L_2 are magnetized with a constant slope. In mode III, inductors L, L_1 and L_2 are demagnetized with a constant slope. It is also observed that the current through inductors L, L_1 and L_2 are 4.78A, 4.74A, and 4.73A, respectively. The voltage waveform across capacitors C_1, C_2, and C_o and the input current waveform are shown in Fig. 8(c).

It is observed that the voltage across capacitor C_1 and C_2 are equal to the input voltage. The voltage across capacitor C_o is equal to the output voltage, i.e. 400.4V. The output voltage and voltage waveform across diodes D_1, D_2 and D are shown in Fig. 8(d). It is observed that peak inverse voltage across diode D_1 is D_2 are −133.7V and −133.4V, respectively.

TABLE 2. Specification of the converter.

Parameters	Values
Input voltage	36-44V
Output voltage	400V
Output Power	500W
Number of A2P-IL	2
Switching frequency	50 kHz
Inductors L, L_1, L_2	700μH/ 10A
Capacitors C_1, C_2, C_o	220uF/50V, 220uF/450V
Diode D_1, D_2, D, D_o	MUR1520G, MUR1520G, MBRF1060, BYV29-500-127
Switches S, S_1, S_2, S_o	IRF250, IRF250, IRF 450V, IRF 450V.

The peak inverse voltage across diode D is −400.5V. The voltage across switches S, S_1, S_2, and S_o is shown in Fig. 8(e). The maximum voltage across S, S_1, S_2 and S_o are 133.9V, 133.6V, 267.1V, and 400.2V, respectively.

Experimental work is carried out to investigate the practical performance of the proposed TM-A2P-IL converter. The experimental parameters are given in Table 2. The reference output voltage is set at 400V. Fig. 9(a) shows the experimentally observed waveform of input voltage, input
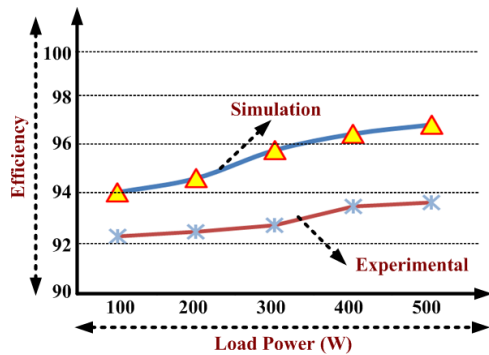
FIGURE 10. Efficiency plot for different power level.

current, output voltage and output current. It is observed that the input voltage is boosted from 40.9V to 400.2V. The input current is found to be 13.03A while the output current is found to be 1.25A. Fig. 9(b) shows the experimentally observed currents waveforms of inductors L, L_1 and L_2 along with output voltage. The inductor currents are continuous, and average current through inductors L, L_1 and L_2 are 4.95A, 4.87A, and 4.85A, respectively. The experimentally observed voltage across capacitor C_1, C_2 and C_o are shown in Fig. 9(c). The voltage across capacitors C_1, C_2 and C_o are 39.8V, 39.2V, and 400.3V. Fig. 9(d) shows the voltage waveform across diodes D_1, D_2 and D. The peak inverse voltages across diodes D_1, D_2, and D are -133.9V, -133.1V, and -400.8V, respectively. The voltage across switches S, S_1, S_2, and S_o are presented in Fig. 9(e). The maximum voltage across S, S_1, S_2 and S_o are 135.2V, 134.8V, 267.3V, and 400.9V, respectively. Several experimental tests are carried out by considering the different power level to investigate the efficiency of the proposed converter. The efficiency plot for different power level is shown in Fig. 10. It is found that the practical efficiency of the converter is 93.86% at 500W.

V. CONCLUSION

A new high gain converter called "Triple mode Active Passive Parallel Intermediate Links" (TM-A2P-IL) converter is proposed for DC microgrid applications. The classical boost converter is modified, and Active Passive Parallel Intermediate Links (A2P-IL) incorporated to achieve high voltage gain. Each A2P-IL leg is a combination of an inductor, capacitor, diode and control switch. The proposed converter operates in three modes and offers a high voltage gain and flexibility in the selection of duty cycle. The detail mode of operation, voltage gain, and boundary for CCM and DCM, design of converter is presented. The proposed converter compared with recently available converter, the proposed converter provides an option to select the number of stages with flexibility in selection duty cycles to achieve high voltage gain. Simulation and experimental results are presented which validate the theoretical analysis and functionality of the proposed converter. The efficiency of the proposed converter is 93.86% at 500W.

ACKNOWLEDGMENT

REFERENCES

[1] Y. P. Siwakoti, F. Blaabjerg, and P. C. Loh, "High step-up trans-inverse (Tx^{-1}) DC–DC converter for the distributed generation system," *IEEE Trans. Ind. Electron.*, vol. 63, no. 7, pp. 4278–4291, Jul. 2016.

[2] L. Meng, Q. Shafiee, G. F. Trecate, H. Karimi, D. Fulwani, X. Lu, and J. Guerrero, "Review on control of DC microgrids and multiple microgrid clusters," *IEEE J. Emerg. Sel. Topics Power Electron.*, vol. 5, no. 3, pp. 928–948, Sep. 2017.

[3] A. Iovine, S. B. Siad, G. Damm, E. De Santis, and M. D. Di Benedetto, "Nonlinear control of a DC MicroGrid for the integration of photovoltaic panels," *IEEE Trans. Autom. Sci. Eng.*, vol. 14, no. 2, pp. 524–535, Apr. 2017.

[4] Y. Yang, Y. Qin, S.-C. Tan, and S. Y. R. Hui, "Efficient improvement of photovoltaic-battery systems in standalone DC microgrids using a local hierarchical control for the battery system," *IEEE Trans. Power Electron.*, vol. 34, no. 11, pp. 10796–10807, Nov. 2019.

[5] S. Kolluri and N. L. Narasamma, "A new isolated auxiliary current pump module for load transient mitigation of isolated/nonisolated step-up/step-down DC–DC converter," *IEEE Trans. Power Electron.*, vol. 30, no. 10, pp. 5991–6000, Oct. 2015.

[6] S. Kenzelmann, A. Rufer, D. Dujic, F. Canales, and Y. R. de Novaes, "Isolated DC/DC structure based on modular multilevel converter," *IEEE Trans. Power Electron.*, vol. 30, no. 1, pp. 89–98, Jan. 2015.

[7] M. Kim and S. Choi, "A fully soft-switched single switch isolated DC–DC converter," *IEEE Trans. Power Electron.*, vol. 30, no. 9, pp. 4883–4890, Sep. 2015.

[8] K. I. Hwu and Y. T. Yau, "High step-up converter based on coupling inductor and bootstrap capacitors with active clamping," *IEEE Trans. Power Electron.*, vol. 29, no. 6, pp. 2655–2660, Jun. 2014.

[9] T.-F. Wu, Y.-S. Lai, J.-C. Hung, and Y.-M. Chen, "Boost converter with coupled inductors and buck–boost type of active clamp," *IEEE Trans. Ind. Electron.*, vol. 55, no. 1, pp. 154–162, Jan. 2008.

[10] A. Alzahrani, M. Ferdowsi, and P. Shamsi, "A family of scalable non-isolated interleaved DC–DC boost converters with voltage multiplier cells," *IEEE Access*, vol. 7, pp. 11707–11721, 2019.

[11] A. Iqbal, M. S. Bhaskar, M. Meraj, S. Padmanaban, and S. Rahman, "Closed-loop control and boundary for CCM and DCM of nonisolated inverting Nx multilevel boost converter for high-voltage step-up applications," *IEEE Trans. Ind. Electron.*, vol. 67, no. 4, pp. 2863–2874, Apr. 2020.

[12] M. S. Bhaskar, P. Sanjeevikumar, J. K. Pedersen, J. B. Holm-Nielsen, and Z. Leonowicz, "XL converters-new series of high gain DC–DC converters for renewable energy conversion," in *Proc. IEEE Int. Conf. Environ. Electr. Eng., IEEE Ind. Commercial Power Syst. Eur. (EEEIC/I&CPS Europe)*, Genova, Italy, Jun. 2019, pp. 1–6.

[13] M. Bhaskar, S. Padmanaban, and J. B. Holm-Nielsen, "Double stage double output DC–DC converters for high voltage loads in fuel cell vehicles," *Energies*, vol. 12, no. 19, p. 3681, Jan. 2019.

[14] D. S. Wijeratne and G. Moschopoulos, "Quadratic power conversion for power electronics: Principles and circuits," *IEEE Trans. Circuits Syst. I, Reg. Papers*, vol. 59, no. 2, pp. 426–438, Feb. 2012.

[15] O. Lopez-Santos, L. Martinez-Salamero, G. Garcia, H. Valderrama-Blavi, and D. A. Zambrano-Prada, "Steady-state analysis of inductor conduction modes in the quadratic boost converter," *IEEE Trans. Power Electron.*, vol. 32, no. 3, pp. 2253–2264, Mar. 2017.

[16] M. S. Bhaskar, S. Padmanaban, F. Blaabjerg, and P. W. Wheeler, "An improved multistage switched inductor boost converter (improved M-SIBC) for renewable energy applications: A key to enhance conversion ratio," in *Proc. IEEE 19th Workshop Control Modeling Power Electron. (COMPEL)*, Padua, Italy, Jun. 2018, pp. 1–6.

[17] J. Yang, Z. He, H. Pang, and G. Tang, "The hybrid-cascaded DC–DC converters suitable for HVdc applications," *IEEE Trans. Power Electron.*, vol. 30, no. 10, pp. 5358–5363, Oct. 2015.

[18] Y.-C. Hsieh, T.-C. Hsueh, and H.-C. Yen, "An interleaved boost converter with zero-voltage transition," *IEEE Trans. Power Electron.*, vol. 24, no. 4, pp. 973–978, Apr. 2009.

[19] M. S. Bhaskar, D. J. Almakhles, S. Padmanaban, F. Blaabjerg, U. Subramaniam, and D. M. Ionel, "Analysis and investigation of hybrid DC–DC non-isolated and non-inverting Nx interleaved multilevel boost converter (Nx-IMBC) for high voltage step-up applications: Hardware implementation," *IEEE Access*, vol. 8, pp. 87309–87328, 2020.

[20] M. S. Bhaskar, M. Meraj, A. Iqbal, and S. Padmanaban, "Nonisolated symmetrical interleaved multilevel boost converter with reduction in voltage rating of capacitors for high-voltage microgrid applications," *IEEE Trans. Ind. Appl.*, vol. 55, no. 6, pp. 7410–7424, Nov. 2019.

[21] B. P. Baddipadiga and M. Ferdowsi, "A high-voltage-gain DC–DC converter based on modified dickson charge pump voltage multiplier," *IEEE Trans. Power Electron.*, vol. 32, no. 10, pp. 7707–7715, Oct. 2017, doi: 10.1109/TPEL.2016.2594016.

[22] M. S. Bhaskar, S. Padmanaban, F. Blaabjerg, L. E. Norum, and A. H. Ertas, "4Nx non-isolated and non-inverting hybrid interleaved multilevel boost converter based on VLSIm cell and cockroft walton voltage multiplier for renewable energy applications," in *Proc. IEEE Int. Conf. Power Electron., Drives Energy Syst. (PEDES)*, Trivandrum, India, Dec. 2016, pp. 1–6.

[23] M. Forouzesh, Y. P. Siwakoti, S. A. Gorji, F. Blaabjerg, and B. Lehman, "A survey on voltage boosting techniques for step-up DC–DC converters," in *Proc. IEEE Energy Convers. Congr. Expo. (ECCE)*, Milwaukee, WI, USA, Sep. 2016, pp. 1–8.

[24] M. Bhaskar, S. Padmanaban, and F. Blaabjerg, "A multistage DC–DC step-up self-balanced and magnetic component-free converter for photovoltaic applications: Hardware implementation," *Energies*, vol. 10, no. 5, p. 719, May 2017.

[25] A. Iqbal, M. S. Bhaskar, M. Meraj, and S. Padmanaban, "DC-transformer modelling, analysis and comparison of the experimental investigation of a non-inverting and non-isolated Nx multilevel boost converter (Nx MBC) for low to high DC voltage applications," *IEEE Access*, vol. 6, pp. 70935–70951, 2018.

[26] M. S. Bhaskar, R. Al-Ammari, M. Meraj, A. Iqbal, and S. Padmanaban, "Modified multilevel buck–boost converter with equal voltage across each capacitor: Analysis and experimental investigations," *IET Power Electron.*, vol. 12, no. 13, pp. 3318–3330, Nov. 2019.

[27] S. Padmanaban, M. Bhaskar, F. Blaabjerg, and Y. Yang, "A new DC–DC multilevel breed of XY converter family for renewable energy applications: Ly multilevel structured boost converter," in *Proc. 44th Annu. Conf. IEEE Ind. Electron. Soc.*, Washington, DC, USA, Oct. 2018, pp. 6110–6115.

[28] J. C. Rosas-Caro, J. M. Ramirez, F. Z. Peng, and A. Valderrabano, "A DC–DC multilevel boost converter," *IET Power Electron.*, vol. 3, no. 1, pp. 129–137, Jan. 2010.

[29] Y. He and F. L. Luo, "Analysis of Luo converters with voltage-lift circuit," *IEE Proc.-Electr. Power Appl.*, vol. 152, no. 5, pp. 1239–1252, Sep. 2005.

[30] T.-J. Liang, J.-H. Lee, S.-M. Chen, J.-F. Chen, and L.-S. Yang, "Novel isolated high-step-up DC–DC converter with voltage lift," *IEEE Trans. Ind. Electron.*, vol. 60, no. 4, pp. 1483–1491, Apr. 2013.

[31] X. Zhu, B. Zhang, Z. Li, H. Li, and L. Ran, "Extended switched-boost DC–DC converters adopting switched-capacitor/switched-inductor cells for high step-up conversion," *IEEE J. Emerg. Sel. Topics Power Electron.*, vol. 5, no. 3, pp. 1020–1030, Sep. 2017.

[32] L.-S. Yang, T.-J. Liang, and J.-F. Chen, "Transformerless DC–DC converters with high step-up voltage gain," *IEEE Trans. Ind. Electron.*, vol. 56, no. 8, pp. 3144–3152, Aug. 2009.

[33] S. Sadaf, S. B. Mahajan, M. Meraj, A. Iqbal, and N. Alemadi, "A novel modified switched inductor boost converter with reduced switch voltage stress," *IEEE Trans. Ind. Electron.*, early access, Feb. 5, 2020, doi: 10.1109/TIE.2020.2970648.

[34] M. Lakshmi and S. Hemamalini, "Nonisolated high gain DC–DC converter for DC microgrids," *IEEE Trans. Ind. Electron.*, vol. 65, no. 2, pp. 1205–1212, Feb. 2018.

[35] M. S. Bhaskar, M. Meraj, A. Iqbal, S. Padmanaban, P. K. Maroti, and R. Alammari, "High gain transformer-less double-duty-triple-mode DC/DC converter for DC microgrid," *IEEE Access*, vol. 7, pp. 36353–36370, 2019.

[36] M. S. Bhaskar, R. Alammari, M. Meraj, S. Padmanaban, and A. Iqbal, "A new triple-switch-triple-mode high step-up converter with wide range of duty cycle for DC microgrid applications," *IEEE Trans. Ind. Appl.*, vol. 55, no. 6, pp. 7425–7441, Nov. 2019.

[37] H. M. Maheri, E. Babaei, M. Sabahi, and S. H. Hosseini, "High step-up DC–DC converter with minimum output voltage ripple," *IEEE Trans. Ind. Electron.*, vol. 64, no. 5, pp. 3568–3575, May 2017.

[38] E. Babaei, H. M. Maheri, M. Sabahi, and S. H. Hosseini, "Extendable nonisolated high gain DC–DC converter based on active-passive inductor cells," *IEEE Trans. Ind. Electron.*, vol. 65, no. 12, pp. 9478–9487, Dec. 2018.

MAHAJAN SAGAR BHASKAR (Senior Member, IEEE) received the bachelor's degree in electronics and telecommunication engineering from University of Mumbai, Mumbai, India, in 2011, the master's degree in power electronics and drives from the Vellore Institute of Technology, VIT University, India, in 2014, and the Ph.D. degree in electrical and electronic engineering from the University of Johannesburg, South Africa, in 2019. He worked as a Research Student with the Power Quality Research Group, Department of Electrical Power Engineering, Universiti Tenaga Nasional (UNITEN), Kuala Lumpur, Malaysia, in August/September 2017. He worked as a Research Assistant with the Department of Electrical Engineering, Qatar University, Doha, Qatar, in 2018 and 2019. He was a Postdoctoral Researcher with his Ph.D. Tutor with the Department of Energy Technology, Aalborg University Esbjerg, Esbjerg, Denmark, in 2019. He is currently with the Renewable Energy Laboratory, Department of Communications and Networks Engineering, College of Engineering, Prince Sultan University, Riyadh, Saudi Arabia. He has authored 100 plus scientific articles particular reference to DC/DC and DC/AC converter, and high gain converter. He is a Senior Member of IEEE Industrial Electronics, Power Electronics, Industrial Application, and Power and Energy, Robotics and Automation, Vehicular Technology Societies, Young Professionals, and various IEEE Councils and Technical Communities. He is a reviewer member of various international journals and conferences, including IEEE and IET. He received the Best Paper Research Paper Awards from IEEE-CENCON'19, IEEE-ICCPCT'14, IET-CEAT'16, and ETAEERE'16 sponsored Lecture note in Electrical Engineering, springer book series. He received the IEEE Access Award Reviewer of Month in January 2019 for his valuable and thorough feedback on manuscripts, and for his quick turnaround on reviews.

DHAFER J. ALMAKHLES (Senior Member, IEEE) received the B.E. degree in electrical engineering from the King Fahd University of Petroleum and Minerals, Dhahran, Saudi Arabia, in 2006, and the master's degree (Hons.) and the Ph.D. degree from The University of Auckland, New Zealand, in 2011 and 2016, respectively. Since 2016, he has been with Prince Sultan University, Saudi Arabia, where is currently the Chairman of the Communications and Networks Engineering Department, and the Director of the Science and Technology Unit and the Intellectual Property Office, Prince Sultan University. He is also the Leader of the Renewable Energy Research Team and Laboratory. He is a reviewer member of various international journals and conferences, including the IEEE and IET. His research interests include power electronics, control theory, unmanned aerial vehicles, renewable energy systems, and FPGA applications. He is a member of the IEEE Power Electronics and the IEEE Control Society.

SANJEEVIKUMAR PADMANABAN (Senior Member, IEEE) received the bachelor's degree in electrical engineering from the University of Madras, Chennai, India, in 2002, the master's degree (Hons.) in electrical engineering from Pondicherry University, Puducherry, India, in 2006, and the Ph.D. degree in electrical engineering from the University of Bologna, Bologna, Italy, in 2012.

He was an Associate Professor with VIT University, from 2012 to 2013. In 2013, he joined the National Institute of Technology Tiruchirappalli, India, as a Faculty Member. In 2014, he was invited as a Visiting Researcher at the Department of Electrical Engineering, Qatar University, Doha, Qatar, funded by the Qatar National Research Foundation (Government of Qatar). He continued his research activities with Dublin Institute of Technology, Dublin, Ireland, in 2014. He was an Associate Professor with the Department of Electrical and Electronics Engineering, University of Johannesburg, Johannesburg, South Africa, from 2016 to 2018. Since 2018, he has been a Faculty Member with the Department of Energy Technology, Aalborg University Esbjerg, Esbjerg, Denmark. He has authored more than 300 scientific articles. He is a Fellow of the Institution of Engineers, India, the Institution of Electronics and Telecommunication Engineers, India, and the Institution of Engineering and Technology, U.K. He was a recipient of the Best Paper cum Most Excellence Research Paper Award from IET-SEISCON'13, IET-CEAT'16, IEEE-EECSI'19, and IEEE-CENCON'19, and five best paper awards from ETAEERE'16 sponsored Lecture Notes in Electrical Engineering, Springer book. He is an Editor/Associate Editor/Editorial Board of refereed journals, in particular the IEEE SYSTEMS JOURNAL, the IEEE TRANSACTIONS ON INDUSTRY APPLICATIONS, IEEE ACCESS, *IET Power Electronics*, and *International Transaction on Electrical Energy Systems*, Wiley, and the Subject Editor of *IET Renewable Power Generation*, *IET Generation, Transmission & Distribution*, and *Obesity Facts* journal, Canada.

A. RAKESH KUMAR (Member, IEEE) received the B.E. degree (Hons.) in electrical and electronics engineering from the DMI College of Engineering, Anna University, Chennai, India, in 2011, the M.Tech. degree in power electronics and drives from the Jerusalem College of Engineering, Anna University, Chennai, in 2013, and the Ph.D. degree from the Vellore Institute of Technology (VIT)–Chennai, in 2020. He worked as an Assistant Professor with the Department of EEE, Rajalakshmi Engineering College, Chennai, from 2013 to 2015. He was working as a Teaching cum Research Assistant with VIT, Chennai, from 2015 to 2019. He is currently a Postdoctoral Fellow with the Department of EEE, National Institute of Technology Tiruchirappalli, Tiruchirappalli, India. His fields of interest include multilevel inverters, inverter modulation techniques, smart grid, and its applications

JENS BO HOLM-NIELSEN received the M.Sc. degree in agricultural systems, crops & soil science, from KVL, Royal Veterinary & Agricultural University, Copenhagen, Denmark, in 1980, and the Ph.D. degree in process analytical technologies for biogas systems from Aalborg University Esbjerg, Esbjerg, Denmark, in 2008. He is currently with the Department of Energy Technology, Aalborg University Esbjerg, and the Head of the Esbjerg Energy Section. He is also the Head of the research group, Center for Bioenergy and Green Engineering established, in 2009. He has vast experience in the field of biorefinery concepts and biogas production–anaerobic digestion. He has implemented projects of bioenergy systems in Denmark with provinces and European states. He was the Technical Advisor for many industries in this field. He has executed many large-scale European Union and United Nation projects in research aspects of bioenergy, biorefinery processes, and the full chain of biogas and green engineering. He has authored more than 300 scientific articles. His current research interests include renewable energy, sustainability, and green jobs for all. He was a member on invitation with various capacities in the committee for over 500 various international conferences and organizer of international conferences, workshops, and training programs in Europe, Central Asia, and China.

SAMSON O. MASEBINU received the bachelor's degree in mechanical engineering from the Federal University of Technology, Akure, Nigeria, in 2011, and the master's degree in chemical engineering technology and the PhD degree in mechanical engineering from the University of Johannesburg, Gauteng, South Africa, in 2015 and 2019, respectively. He undertook his Postdoctoral Research Fellowship at the University of Johannesburg. He is currently an Engineer and a Research Lead for the Process and Energy Engineering Unit, Process, Energy and Environmental Technology Station, University of Johannesburg. He is also a Visiting Researcher, under the DANIDA funding to the Department of Energy Technology, Aalborg University Esbjerg, Esbjerg, Denmark. He received several awards among which are the most outstanding master's research in the faculty of Engineering and the Built Environment, University of Johannesburg, First position in interfaculty 3-mins Ph.D. thesis competition and postdoctoral award of excellence for academic achievement at the University of Johannesburg. He has worked on several projects mainly in the field of renewable energy and environmental sustainability. He has authored more than 35 scientific articles and reports. He is a Registered Member of the Engineering Council of South Africa.

• • •